Earth-Mars Transfers Through Moon Distant Retrograde Orbits

Davide Conte[a,1], Marilena Di Carlo[b], Koki Ho[c], David B. Spencer[a], Massimiliano Vasile[b]

[a] *Department of Aerospace Engineering, The Pennsylvania State University, 229 Hammond Building, University Park, PA 16802, USA*
[b] *Department of Mechanical and Aerospace Engineering, University of Strathclyde, James Weir Building, Glasgow G1 1XJ, United Kingdom*
[c] *Department of Aerospace Engineering, University of Illinois at Urbana-Champaign, 302F Talbot Laboratory, 104 South Wright Street, Urbana, IL 61801, USA*

Abstract

This paper focuses on the trajectory design which is relevant for missions that would exploit the use of asteroid mining in stable cis-lunar orbits to facilitate deep space missions, specifically human Mars exploration. Assuming that a refueling "gas station" is present at a given lunar Distant Retrograde Orbit (DRO), ways of departing from the Earth to Mars via that DRO are analyzed. Thus, the analysis and results presented in this paper add a new cis-lunar departure orbit for Earth-Mars missions. Porkchop plots depicting the required C_3 at launch, v_∞ at arrival, Time of Flight (TOF), and total ΔV for various DRO departure and Mars arrival dates are created and compared with results obtained for low ΔV Low Earth Orbit (LEO) to Mars trajectories. The results show that propellant-optimal trajectories from LEO to Mars through a DRO have higher overall mission ΔV due to the additional stop at the DRO. However, they have lower Initial Mass in LEO (IMLEO) and thus lower gear ratio as well as lower TOF than direct LEO to Mars transfers. This results in a lower overall spacecraft dry mass that needs to be launched into space from Earth's surface.

Keywords: Mars, Mars missions, lunar DRO, Earth-Mars trajectories,

[1] Corresponding author. Email address: davide.conte90@gmail.com

1. Introduction

Lunar Distant Retrograde Orbits (DROs) are orbits that exist due to third-body effects. Such trajectories are the solutions of the Circular Restricted Three Body Problem (CR3BP) of a system in which Earth's and Moon's gravitational attractions are considered. A DRO is possibly a critical stepping stone, both implicitly and literally, for the next big goal in space exploration: human Mars exploration.

The history of exploration has taught mission designers the importance of logistical considerations for such expeditions. Part of the logistics considerations in space exploration includes the locations of on-orbit propellant depots, in-situ resource utilization (ISRU) plants, and other types of space infrastructure [1]. Multiple recent studies have shown the promising effectiveness of having a propellant depot on the way to or back from the destination [2, 3].

Recent interests in asteroid mining and utilizing cis-lunar space as a gateway for deep space robotic and human missions (including Mars missions) have increased the focus on utilizing the Moon and its surrounding as an intermediate step to eventually reach Mars [4, 5]. Recently NASA has announced its plan to build a crew tended spaceport in lunar orbit that would serve as a gateway to deep space and the lunar surface [6]. After the establishment of the Deep Space Gateway, the objective is to develop a transport system for human travel that, from the gateway, would reach destinations beyond the Earth-Moon system, including Mars. In the early 2000s, a halo orbit around the Earth-Moon Lagrange point 1 was proposed as a gateway where to mount lunar and interplanetary missions for the OASIS (Orbital Aggregation and Space Infrastructure Systems) study [7]. Earth and lunar departure orbits are analyzed also in [8], including High Earth Orbits (HEO) with low or high perigee and cis-lunar departure orbits. Such orbits allow spacecraft to obtain the necessary C_3 to reach destinations such as Mars and Near Earth Asteroids (NEA) of interest [8].

A DRO has recently been proposed to be one of the most suitable locations to locate space infrastructure. This is due to its orbital stability and ease of access in terms of gravity well [9, 10]. For example, a propellant depot can be at a DRO so that a cargo mission can visit that depot to be refueled before heading to its destination. In addition, a space station can also be located at a DRO, which can be used as a maintenance base or safe haven for any unexpected contingencies in cis-lunar space. Moreover, a DRO can be used for the assembly of large spacecraft. This idea is attractive because, e.g., one of the many benefits of in-orbit spacecraft assembly is that the final spacecraft size and mass are not affected by launch vehicle constraints.

In order to realize the above scenarios, an efficient transfer orbit from Earth to Mars via a DRO (or the other way around) is critical. The contribution of this work with respect to the studies available in the literature resides in the study of transfers to and from a lunar DRO to reach Mars. An Earth flyby maneuver is used for departing the DRO to leave the Earth-Moon system in order to optimize the use of propellant within the Earth-Moon system. Thus, necessary ΔV, TOF, mass requirements and porkchop plots for a given synodic period are shown in this paper.

The analysis of LEO to DRO and DRO to Mars trajectories was supported by the following assumptions:

- ΔV maneuvers are treated as impulsive maneuvers.
- Earth-Moon dynamics is modelled as the Circular Restricted Three Body Problem (CR3BP) using an Earth-Moon mean distance of 384,400 km.
- Patched conics are used for interplanetary orbital transfers.
- Secular perturbations of other planetary bodies are neglected.

The paper starts with an analysis of the role of DROs in Mars missions in Section 2. Transfers from Earth to DRO and from DRO to Mars are presented in Sections 3 and 4 and Section 5 draw conclusions on this work.

2. The role of DROs in Mars missions

In order to show the value of a DRO for Mars exploration, a simple numerical example is shown in this section. The considered scenarios assume a cargo mission, which can be a habitat pre-deployment mission preceding human missions. A propellant depot is assumed to be located at a DRO, and here the value of having such a propellant depot is analyzed. More precisely, it is of interest to find the mass savings on the Initial Mass in Low Earth Orbit (IMLEO) by refilling the propellant tanks from the depot at a DRO before departing for Mars. Note that the cases with a depot cannot be simply compared against those without a depot because the depot development and launch costs would need to be considered. Instead, the result would give an indication about how much cost the develop and launch of such a propellant depot would be worth considering its reusability.

With the representative ΔV and TOF resulted from later analysis, the following scenarios are considered for a Mars mission.

- Scenario 1. Direct transfer from Earth to Mars: the vehicle directly departs from Earth to Mars.

- Scenario 2. Oxygen refill in DRO: the vehicle departs from Earth to the DRO, refills its oxygen tank from a propellant depot in the DRO, and heads to Mars.

- Scenario 3. Hydrogen and Oxygen Refill in DRO: the vehicle departs from Earth to the DRO, refills its hydrogen and oxygen tanks from a propellant depot in the DRO, and heads to Mars.

Note that for both scenarios 2 and 3, an Earth flyby after departing the DRO is considered. The computation is simply based on the rocket equation [11]. The assumed parameters are shown in Table 1, where LMO stands for Low Mars Orbit, and the results are shown in Table 2. The ΔV and TOF values assume the Earth-Mars synodic period 2035-2036. Chemical engines with a specific impulse (I_{sp}) of 450 s is assumed as the vehicle propulsion system. The

refill operation is assumed to take 10 days. To represent the IMLEO reduction, the gear ratio is shown, which is defined as the ratio of IMLEO to the mass that arrives at Low Mars Orbit (LMO). In addition, the number of launches is shown assuming the equivalent payload as NASA Design Reference Architecture 5.0 cargo pre-deployment mission (40 mT on Martian surface [12]) and the launches by the 130 mT Space Launch System (SLS) Block 2.

Table 1: Assumed parameters

From	To	ΔV [km/s]	TOF [days]
LEO	LMO	5.76	202
LEO	DRO	3.82	6
DRO	LMO	3.29	206

Table 2: ΔV and TOF for each case

Scenario	Gear Ratio	TOF [days]	SLS launches
1	13.09	202	5
2	10.56	222	4
3	8.43	222	3

The results show that stopping at the DRO "gas station" would provide the propellant necessary for part or all of the rest of the journey to Mars, which would effectively reduce the propellant mass and the size (and therefore mass) of the tanks that need to be launched from Earth. Thus, a smaller number of launches or smaller rockets could be used for the same payload mass to be sent to Mars. In the above case, the total spacecraft mass can be reduced by more than 35%, so the number of launches can be reduced from five to three, which can save on launch cost and time significantly. (Note that the current schedule for SLS launch frequency is only once a year.)

An example scenario of utilization of propellant depot in a DRO and lunar ISRU for a Mars cargo mission is shown in Figure 1. The first launch is a crewed mission that delivers the ISRU plant to the lunar surface and the propellant depot to a DRO. During the ISRU operation period, the human crew maintains the ISRU plant and performs science missions at the same time on the lunar

surface. After the ISRU propellant generation, the obtained propellant is delivered to the propellant depot in the DRO, and the human crew returns to Earth. In the meantime, the Mars cargo is launched and assembled in LEO, stops in a DRO to get refilled, and heads to Mars to deliver the cargo (e.g. habitat pre-deployment for later crew missions). Note that in this scenario, the propellant depot is assumed to be refilled by ISRU, but there are other possibilities for the usage of propellant depots [3]. This scenario provides an example of how DROs can be used for Mars exploration, which thus motivates this research to design trajectories around a DRO.

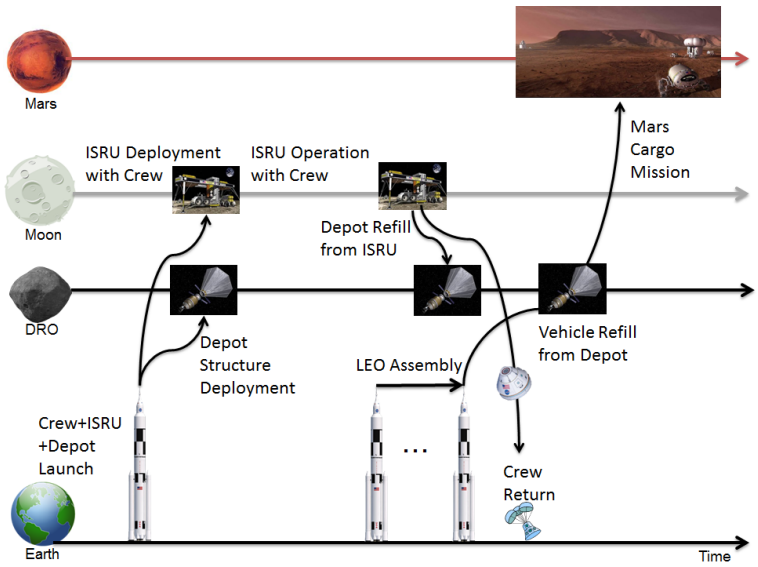

Figure 1: Concept of Operations (ConOps) for an example scenario of using DRO (Icon Credit: NASA, ULA)

3. Earth - Lunar DRO Transfer

No closed form solution for the DRO in the CR3BP exists. A collection of positions and velocities for points along the orbit can however be obtained by implementing a shooting method. The shooting method propagates the motion of a point in the CR3BP from one of the approximate initial conditions (position

and velocities) that can be derived from reference [13]. In particular, the initial position's components are $x \neq 0$ and $y = 0$ and the velocity's components are $v_x = 0$ and $v_y \neq 0$, in the CR3BP rotating reference frame. The exact values of the initial conditions for the position and velocities are obtained from the shooting method imposing that, after one orbital period, a periodic orbit is obtained. In Figure 2 and Figure 3 a lunar DRO of 61,500 km amplitude is represented in the rotating reference frame of the CR3BP and in the inertial reference frame centered at the Earth. In Figure 2 the x-axis points to the Moon and the y-axis is perpendicular to it and both lie in the Earth-Moon plane. In Figure 3 the x and y axes lie on an inertial plane centered at the Earth-Moon barycenter. An amplitude of 61,500 km was chosen for the DRO based on the work done at the Caltech Space Challenge 2015 and due to its long-term stability [14, 9].

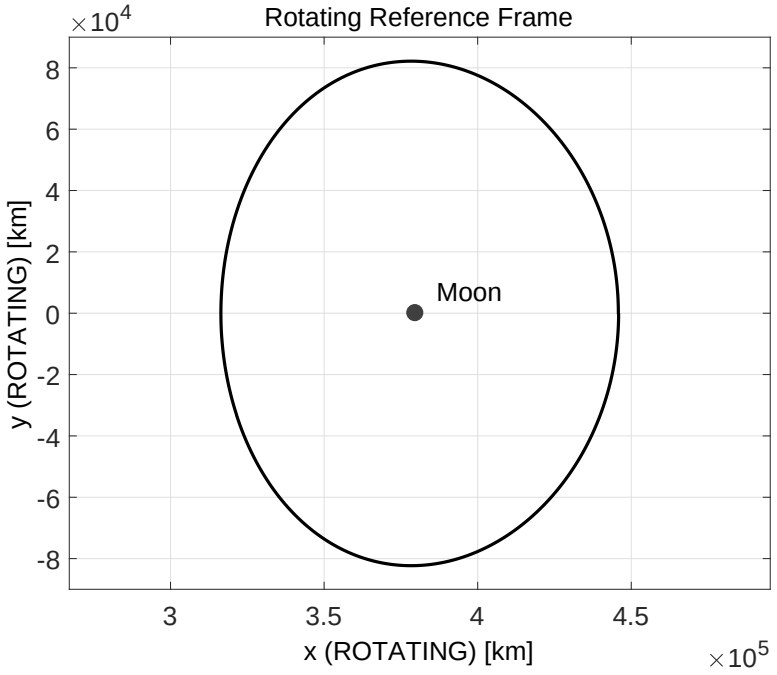

Figure 2: 61,500 km amplitude DRO in the rotating Earth-Moon reference frame

The orbit selection process for the transfer from Earth to lunar DRO often

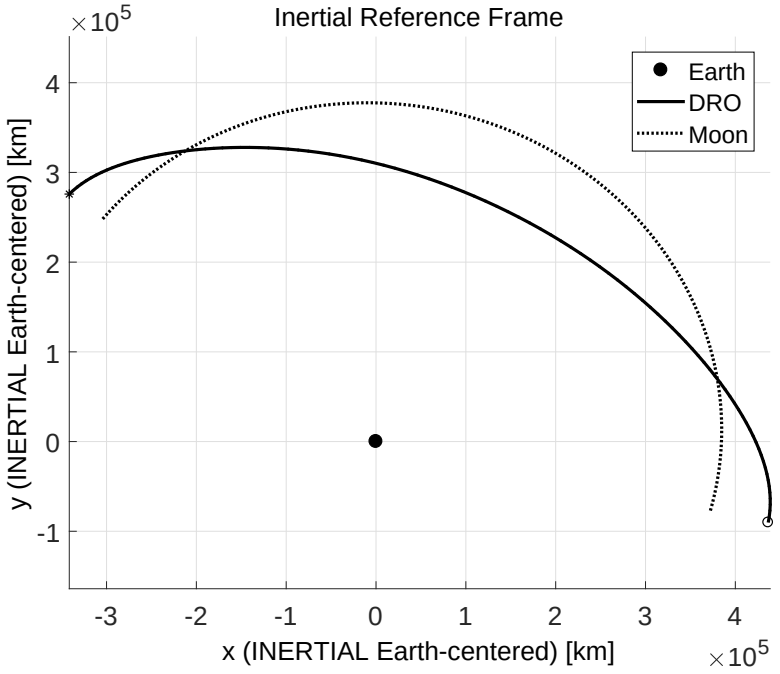

Figure 3: 61,500 km amplitude DRO in the inertial Earth-centered reference frame

comes to the trades between ΔV and TOF. Human missions typically prefer a trajectory with a short TOF even if ΔV is not minimized. This is due to crew health problems such as radiation dose limits and other physiological and psychological problems. Chemical propulsion systems are often used for such missions. This trend is true for part of the robotic missions that requires a fast delivery as well. Most robotic missions, on the other hand, typically prefer a trajectory with a small ΔV even though their TOF is longer. For these missions, a low-thrust electric propulsion system or low-energy transfers with ballistic captures (e.g. weak stability boundary transfers [15]) may be preferred to save propellant. For fast human missions, where a high thrust propulsion system (e.g. chemical) is preferred, the following transfer types have been considered:

- Direct transfer with lunar far side injection. This transfer requires two maneuvers, one to depart from LEO and one to insert into the DRO [16],

with the injection occurring tangentially along the x-axis of the Earth-Moon rotating reference frame. This transfer is shown in Figure 4.

- Prograde or retrograde powered lunar gravity assist. These transfers requires three maneuvers: departure from LEO, periselenium maneuver and injection maneuver, which can occur either with a prograde or retrograde motion. Retrograde transfers are typically less expensive in terms of injection ΔV [13].

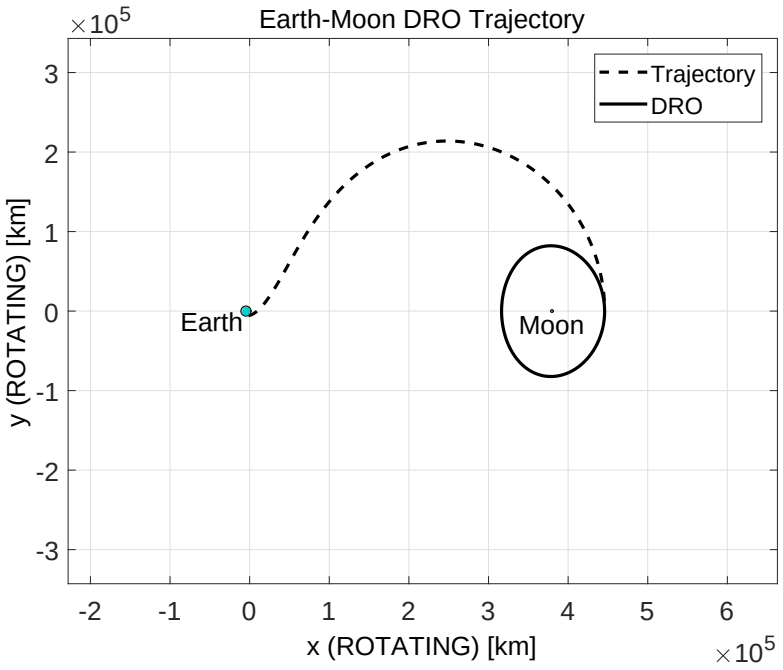

Figure 4: Direct Earth-DRO transfer

A direct transfer was chosen because of the reduced TOF and number of critical manuevers that the vehicle must perform [17]. The direct transfer from Earth to the DRO takes 5.86 days; it requires a burnout velocity in LEO of 10.91 km/s and a ΔV for the injection into the DRO of approximately 620 m/s.

4. Lunar DRO - Mars Transfer

In order to know the characteristic energy (C_3) the spacecraft needs to achieve to leave the Earth-Moon system and arrive at Mars at a certain arrival date, Earth-Mars porkchop plots were generated. The abscissa and ordinate on a porkchop plot represent the Earth-Moon departure and Mars arrival dates, respectively. The key parameters that are plotted on porkchop plots and used to investigate possible transfer orbits are the Earth departure characteristic energy, C_3, the Mars arrival v_∞, and TOF. These parameters are plotted as contour lines of constant values and allow mission designers to decide the best launch and arrival windows for interplanetary missions. Figure 5 shows an example of a porkchop plot for Earth-Mars transfers during the 2035-2036 synodic period. Note that, in this paper, C_3 values are not sufficient for the mission design presented and therefore vectors of C_3, i.e. $\vec{C_3}$, are used.

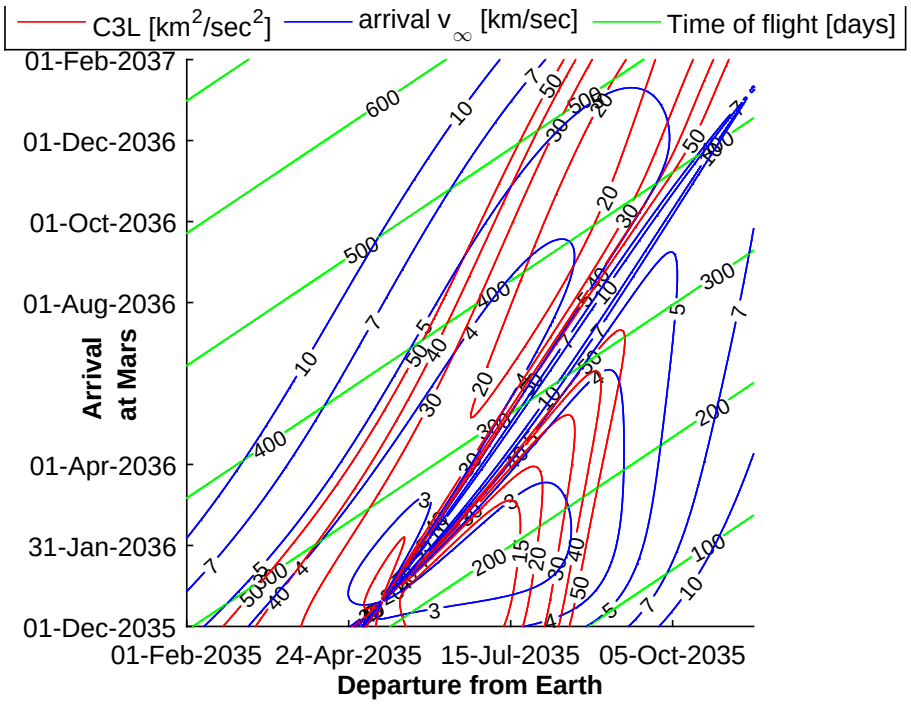

Figure 5: Porkchop plot illustrating Earth-Mars transfer for the 2035-2036 timeframe.

Figure 5 shows departure maneuvers for any dates falling within the time period that was considered (February 1, 2035 to November 15, 2035) while in reality one must take into account the geometry of the Earth and the Moon. Thus, $\vec{C_3}$ vectors were transformed from the J2000 Ecliptic (Ecl) frame to the Earth-Moon rotating reference frame. Such transformation was done by using the following Direction Cosine Matrices [11]:

- $R^{Ecl-EME}$: transforms from J2000 Ecliptic to Earth Mean Equatorial (EME) frame using the obliquity of the Earth, $\varepsilon_{\oplus} = 23.43928$ deg.
- $R^{EME-EMI}$: transforms from EME to Earth-Moon Inertial (EMI) perifocal frame using the inclination, right ascension of the ascending node, and argument of periapsis of the Moon's orbit derived from its ephemeris.
- $R^{EMI-EMR}$: transforms from EMI to Earth-Moon Rotating (EMR) reference frame using the true anomaly of the Moon's orbit derived from its ephemeris.

Consequently, $\vec{C_3}$ vectors can be converted from Ecl to EMR using the relationship:

$$\vec{C}_3^{EMR} = R^{EMI-EMR} R^{EME-EMI} R^{Ecl-EME} \vec{C}_3^{Ecl} \tag{1}$$

Using Eq. (1) and the resulting $\vec{C}_3^{EMR}$, right ascension α and declination δ of departure $\vec{C_3}$ vectors can be computed. Right ascension and declination are defined in the EMR frame as shown in Figure 6.

$\vec{C_3}$ changes for each Earth departure date and Mars arrival date combination. Thus, from Eq. (1) it is possible to calculate right ascension and declination for each $\vec{C_3}$ as a function of departure and arrival dates. Figure 7 and Figure 8 show such time-dependent relationship for right ascension and declination respectively.

While right ascension varies almost uniformly from 0 to 360 degrees roughly once per month, declination is less predictable. On the other hand, right ascension is a limiting factor for Earth-Moon departures to Mars because the correct

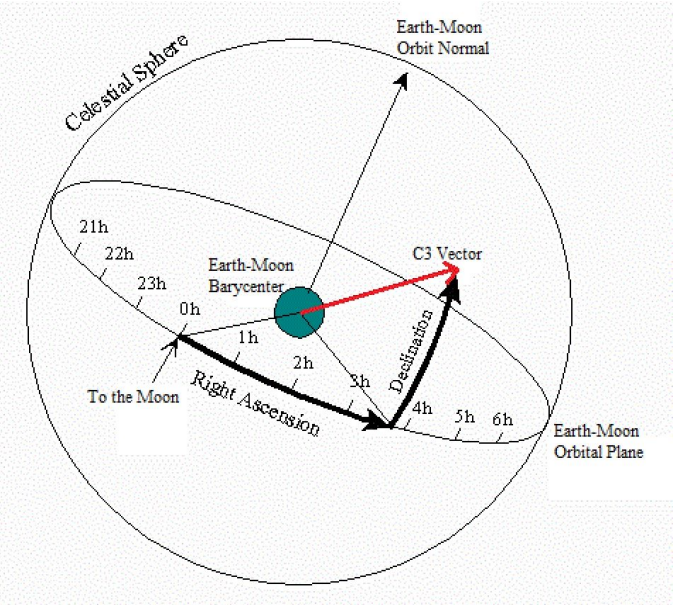

Figure 6: Geometry of Right Ascension and Declination of departure C3 vectors [18].

alignment that permits a spacecraft to leave on the correct Mars departure hyperbolic trajectory asymptote occurs only for about two consecutive days per month. Declination can significantly influence the required departure ΔV but it does not represent a limiting factor in terms of timing.

In order to optimize the use of ΔV when leaving the Earth-Moon system, a flyby of Earth was considered. In fact, performing a ΔV when going near perigee optimizes the use of propellant since the spacecraft is going at its fastest speed. Thus, the Mars departure maneuver consists of the DRO departure and the maneuver that is performed during the Earth flyby.

Therefore, one must compute ΔV for Mars departure by adding both DRO-Earth and Earth flyby propulsive maneuvers. An Earth flyby altitude of 300 km was chosen to avoid atmospheric drag and to maintain the spacecraft at a safe distance from the Earth's surface. Starting from a combination of departure and arrival dates, $\vec{C}_3$ magnitudes and orientation (α and δ) were determined as mentioned previously. Using the given Earth flyby altitude of 300 km and $\vec{C}_3$

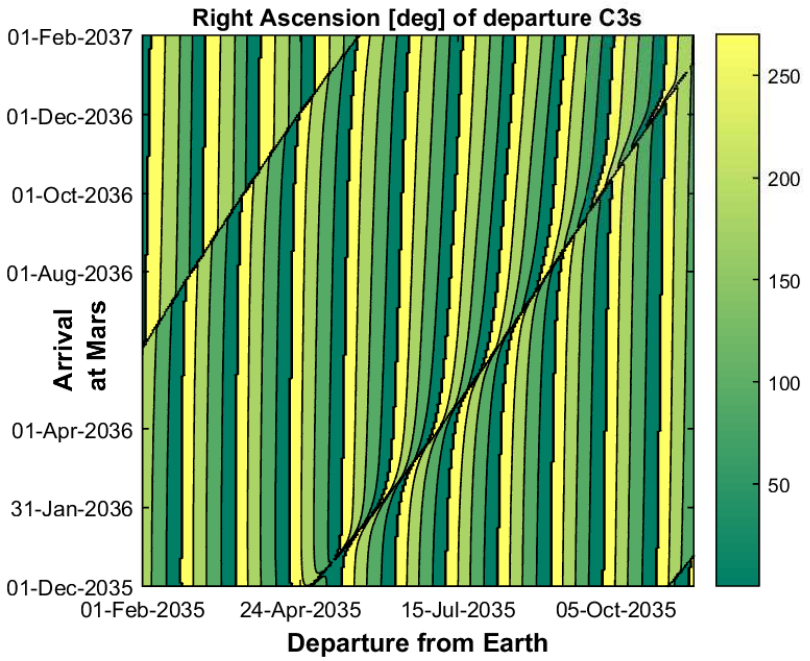

Figure 7: Right ascension (in degrees) of departure $\vec{C}_3$ vectors for the 2035-2036 Earth-Mars synodic period.

magnitude, one can calculate the perigee velocity a spacecraft needs ($v_{p,n}$) in order to achieve such C_3. Right ascension α provides information on whether or not a departure trajectory exists based on the Earth-Moon geometry. Taking into account the TOF from DRO to Earth and the TOF from perigee to the Earth's Sphere Of Influence (SOI), it was found that α values falling in the range of approximately 205 to 240 degrees yield feasible trajectories two days every month as explained previously. The right ascension α of the vector $\vec{C}_3$ can be related to the right ascension θ of the spacecraft perigee in its trajectory from the DRO to the Earth (Figure 9). In Figure 9, $\gamma/2$ represents half of the turn angle (γ) due to the flyby.

In particular, the value of θ depends on the departure point on the DRO for the DRO-Earth transfer. Different points on the DRO, all characterized by $x \geq r_{EM}$, where r_{EM} is the Earth moon distance, were considered. A shooting

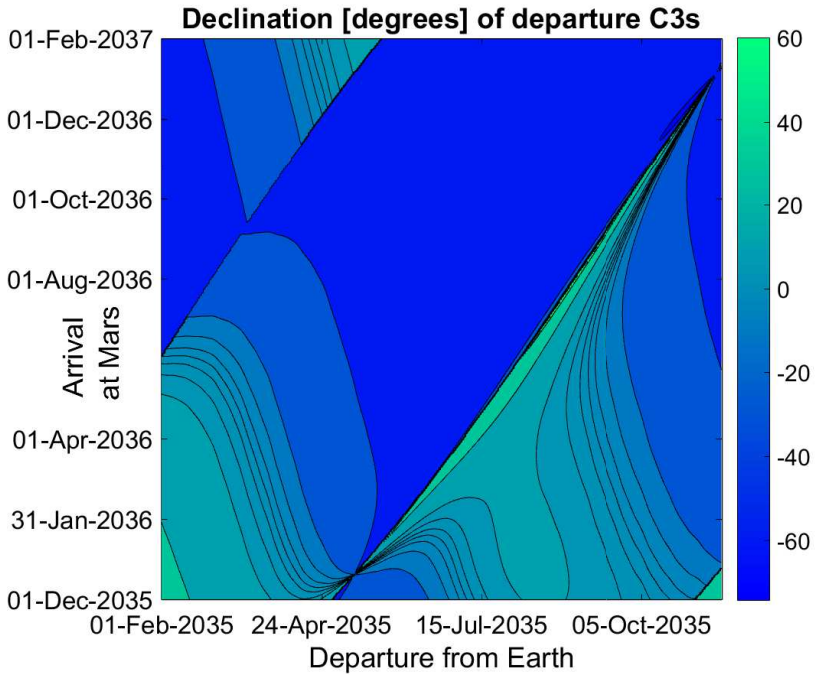

Figure 8: Declination (in degrees) of departure $\vec{C}_3$ vectors for the 2035-2036 Earth-Mars synodic period.

method was implemented to define the departure ΔV leading to a trajectory with perigee altitude of 300 km. The results obtained, in terms of ΔV and TOF from the DRO to the Earth perigee, are shown in Figure 10 for different departure positions on the DRO, identified by their y-values. The corresponding v_p (velocity at perigee) and θ (right ascension of the perigee) values for each departure position were also computed (Figures 11).

The relationship between θ and α is (Figure 9):

$$\theta = \alpha - 90^\circ - \arcsin\left[\left(\frac{r_p}{\mu} v_{p,n}^2 - 1\right)^{-1}\right] + \frac{TOF_{hyp}}{T_{EM}}(360^\circ) \tag{2}$$

where r_p is the perigee radius of the Earth flyby, $v_{p,n}$ is the perigee velocity the spacecraft needs at r_p in order to achieve the given C_3, TOF_{hyp} is the TOF of the departure hyperbolic orbit from r_p to the Earth's SOI and T_{EM}

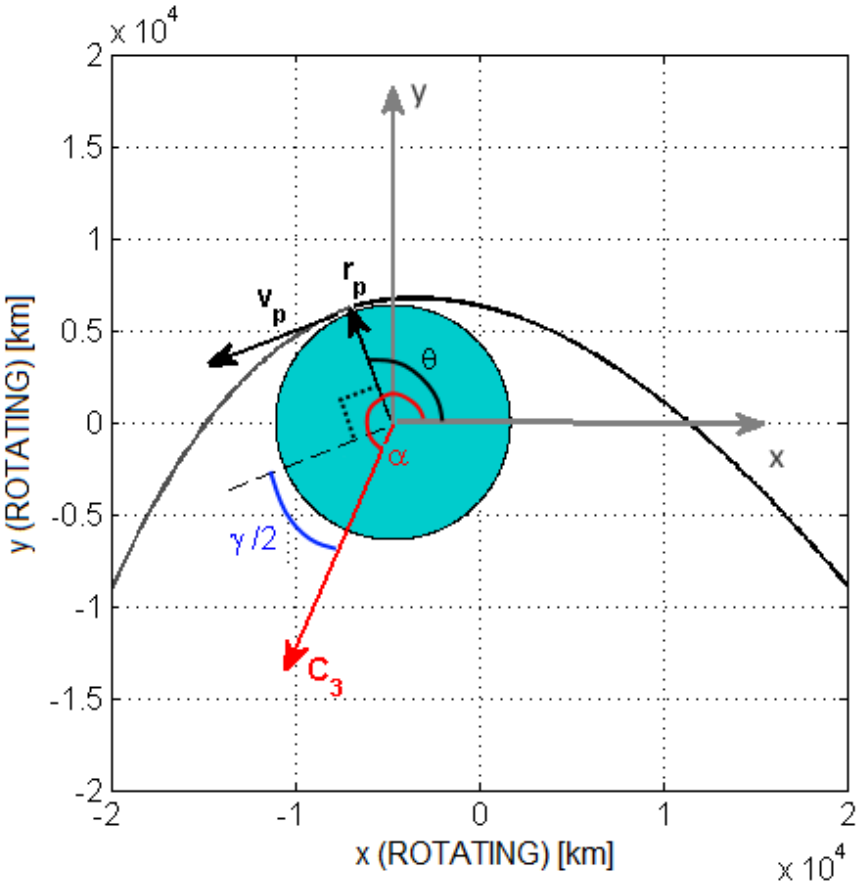

Figure 9: Geometry of the Earth flyby.

is the Earth-Moon orbital period. Note that the term $\arcsin\left[\left(\frac{r_p}{\mu}v_{p,n}^2 - 1\right)^{-1}\right]$ represents half of the turn angle γ obtained from the Earth flyby maneuver and the term $(TOF_{hyp})/T_{EM}(360^\circ)$ takes into account the rotation of the Earth-Moon rotating reference frame while the spacecraft is escaping the Earth-Moon system.

Once $v_{p,n}$ and v_p are found, ΔV_{EF}, i.e. the Earth flyby ΔV, can be computed using the law of cosines:

$$\Delta V_{EF} = \sqrt{v_p^2 + v_{p,n}^2 - 2v_p v_{p,n}\cos\delta} \tag{3}$$

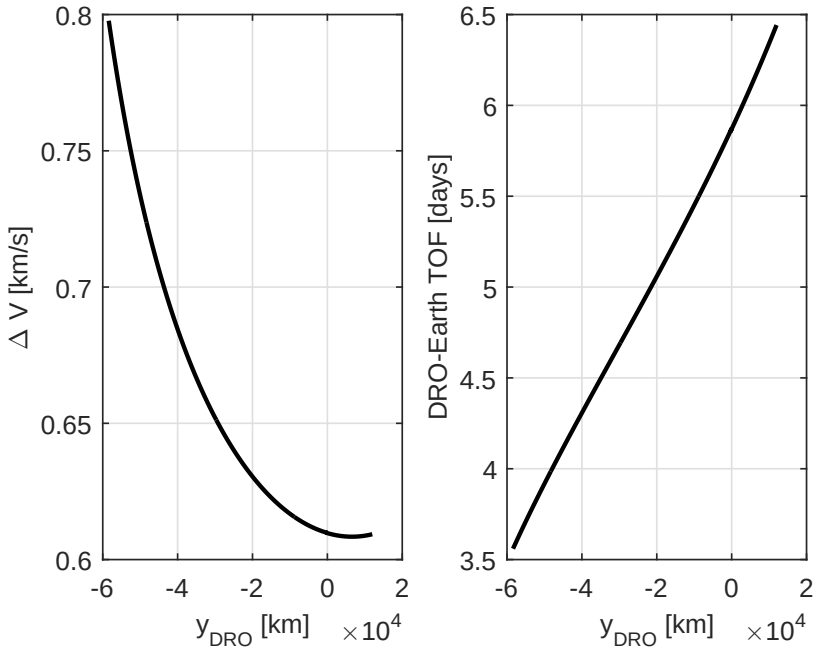

Figure 10: ΔV and TOF from a DRO as function of the departure point on the DRO.

Therefore, ΔV_{dep}, i.e. the departure ΔV, can be computed as follows:

$$\Delta V_{dep} = \Delta V_{DRO} + \Delta V_{EF} \tag{4}$$

while ΔV_{tot}, i.e. the total ΔV needed from leaving the DRO to arriving into a LMO, is defined as:

$$\Delta V_{tot} = \Delta V_{dep} + \Delta V_{MOI} \tag{5}$$

where ΔV_{MOI} is the ΔV needed to perform a Mars Orbit Insertion (MOI) at a parking orbit of 200x200 km altitude.

Figure 12 shows an example of feasible departure C_3 vectors in the EMR frame. Table 3 summarizes the key parameters for such departure opportunities using an Earth flyby altitude of 300 km. Note that this is an example and it is not optimized. Propellant-optimal trajectories are explained later and presented in Tables 4 and 5.

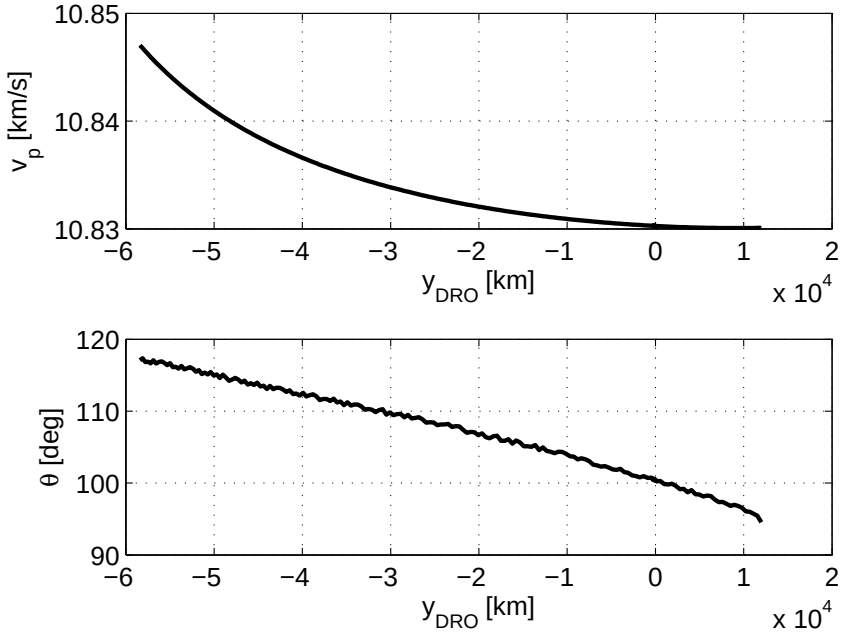

Figure 11: Velocity v_p and right ascension θ at Earth perigee, v_p.

Table 3: Key parameters for the example of departure opportunities shown in Figure 12.

Parameter	Minimum Value	Maximum Value
Departure Dates	July 19, 2035	July 20, 2035
Arrival Dates	January 14, 2036	February 8, 2036
C_3 at Launch [km^2/s^2]	14.683	15.8523
α [deg]	204.97	226.96
δ [deg]	9.041	10.278
ΔV_{dep} [km/s]	2.5783	2.8705

Figure 13 shows a sample trajectory a spacecraft would undertake to leave the DRO and reach the Earth's SOI. Figure 14 and Figure 15 respectively show ΔV_{dep} and ΔV_{tot} for feasible departure trajectories during the 2035-2036 Earth-Mars synodic period. White space means that no feasible departure trajectory exists. ΔV_{tot} was calculated considering a 200x200 km altitude final LMO for all cases. ΔV_{tot} does not take into account the ΔV necessary to reach the DRO from

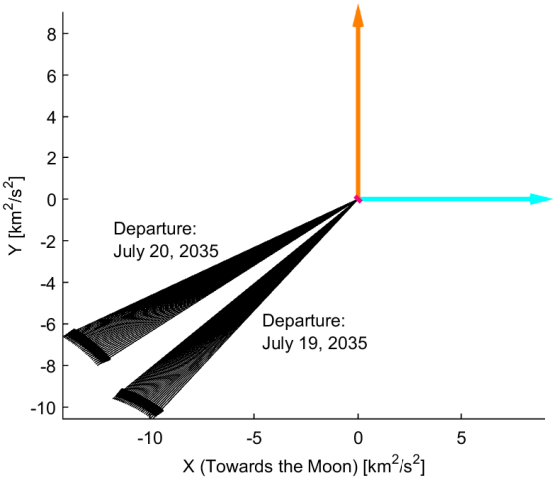

Figure 12: Example of feasible departure C_3 vectors.

LEO; this is because a refueling depot exists in such DRO. In order to maintain ΔV within reasonable values and values that would be and comparable with ΔV maneuvers for direct LEO to LMO, ΔV_{dep} and ΔV_{tot} were constrained to an upper bound of 5 km/s and 9 km/s respectively.

Table 4 summarizes the minimum ΔV_{tot} case for this synodic period and compares the key parameters with a LEO-LMO trajectory [19]. Table 5 summarizes all minimum ΔV_{tot} cases for each Earth-Mars synodic period from 2020 to 2040 and compares ΔV_{tot} and TOF with LEO-LMO trajectories [19]. Absolute lowest ΔV_{tot} for each trajectory type is in bold. From Table 5, it is clear that DRO-LMO maneuvers can save from 1.1 to 2.5 km/s of the ΔV_{tot}. On the other hand, departure opportunities are limited to a maximum of two days roughly every month due to the Earth-Moon-C_3 geometry necessary to achieve the required departure hyperbolic asymptote; additionally, the use of high thrust

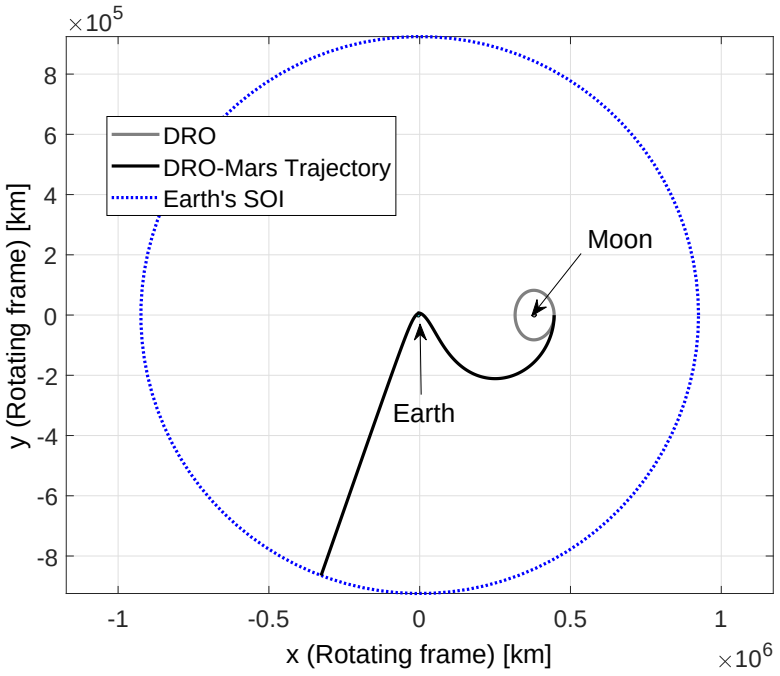

Figure 13: Total transfer.

propulsion is necessary to successfully achieve the required ΔV during the Earth flyby maneuver.

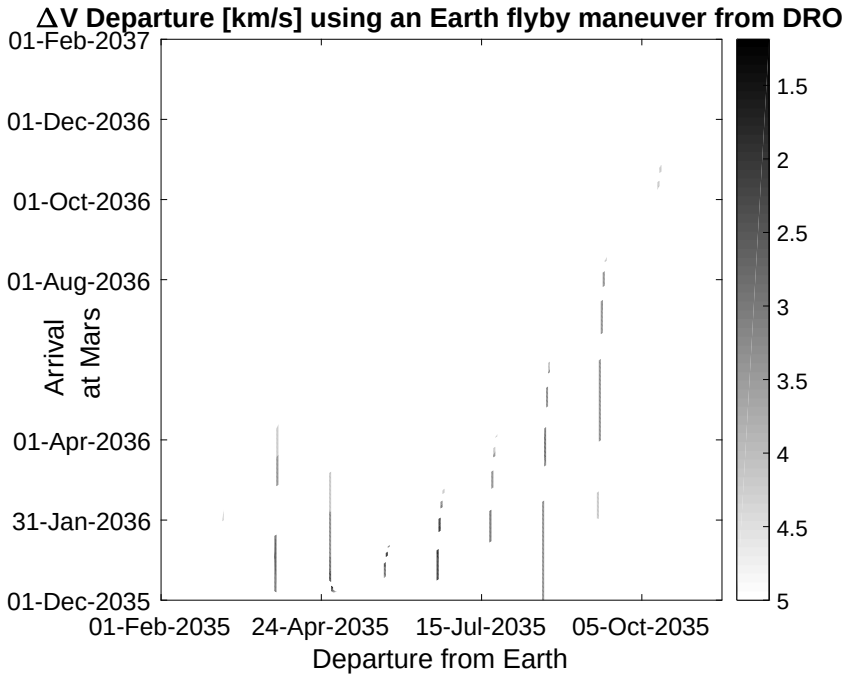

Figure 14: ΔV_{dep} (km/s) for the 2035-2036 Earth-Mars synodic period.

Table 4: Minimum ΔV_{tot} case and comparison with LEO-LMO. [19]

Parameter	Value for DRO-LMO	Value for LEO-LMO
ΔV_{tot} [km/s]	3.2904	5.7582
C_3 at Launch [km^2/s^2]	10.351	10.397
v_∞ at Arrival [km/s]	2.6516	2.6283
Departure Date	June 23, 2035	June 28, 2035
Arrival Date	January 15, 2036	January 16, 2036
Time of Flight [days]	206	202

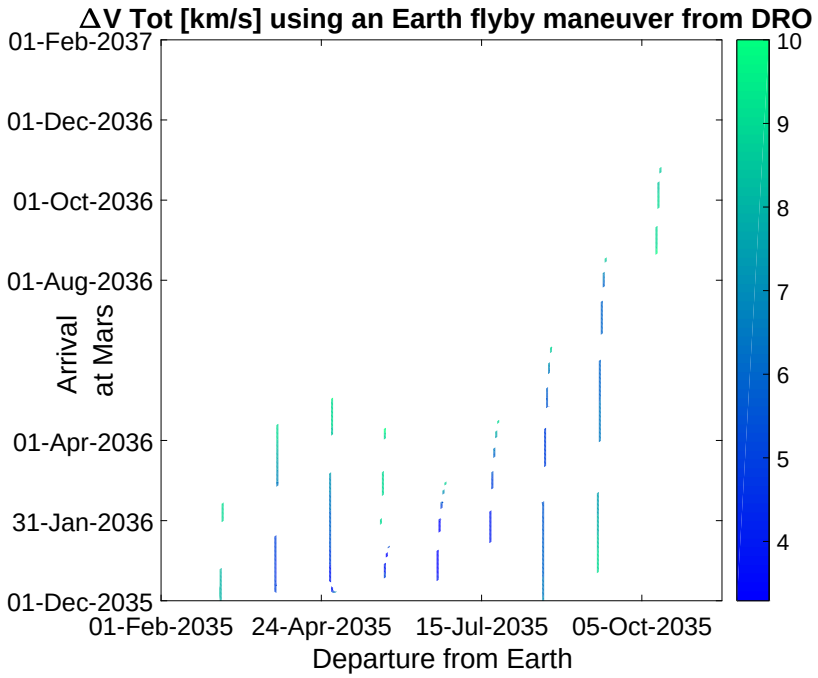

Figure 15: ΔV_{tot} (km/s) for the 2035-2036 Earth-Mars synodic period.

Table 5: ΔV_{tot} and TOF comparison between DRO-LMO and LEO-LMO trajectories [19].

Synodic Period	ΔV_{tot} [km/s] DRO-LMO	TOF [days] DRO-LMO	ΔV_{tot} [km/s] LEO-LMO	TOF [days] LEO-LMO
2020-2021	3.4430	210	5.8921	207
2022-2023	3.8884	241	5.9536	347
2024-2025	3.9823	265	5.7166	333
2026-2027	4.0035	293	**5.6799**	311
2028-2029	3.5863	299	5.8722	300
2030-2031	5.0580	186	6.2268	283
2032-2033	4.0130	229	6.0583	200
2035-2036	**3.2904**	206	5.7582	202
2037-2038	3.8789	240	6.1000	348
2039-2040	4.1087	253	5.7862	340

5. Conclusions

The analysis and results presented in this paper add a new cis-lunar departure orbit, namely from a DRO, to escape the Earth-Moon system and arrive at Mars. DRO-LMO trajectories have the advantage of needing less ΔV_{tot} than LEO-LMO trajectories. Lower ΔV_{tot} means fewer or smaller launch vehicles from Earth, and thus the launch cost is reduced. Additionally, the assembly of large spacecraft in a cis-lunar environment such as a DRO means that the final spacecraft size and mass are not affected by launch vehicle constraints.

A few disadvantages of DRO-LMO trajectories exist. In fact, since the necessary ΔV to depart from the Earth-Moon system starting from a DRO is highly dependent on the position of the Moon with respect to the Earth at departure and the desired interplanetary transfer trajectory to arrive at Mars, DRO-LMO trajectories are limited to roughly a two-day window every month. Additionally, since the Moon's orbital elements change in time, DRO-LMO low ΔV_{tot} opportunities do not repeat as regularly as LEO-LMO low ΔV_{tot} opportunities. Conversely, because Moon DROs possess a much higher orbital energy than LEOs, ΔV_{dep} for DRO-LMO is generally much lower than that for LEO-LMO. Additionally, even though DRO-LMO trajectories require the spacecraft to reach a DRO in the first place and hence add TOF to the total mission duration, DRO-LMO interplanetary TOFs are lower than LEO-LMO interplanetary TOFs and never exceed 300 days for the majority of the cases that are analyzed from 2020 to 2040. Another mission analysis aspect to keep into account is the phasing and rendezvous with the "fuel depot" required prior to departing from Mars. This consideration would need more detailed analysis. In this paper, the "fuel depot" is assumed to already be in the correct position at the time of departure for Mars. In this paper, only a LMO of 200x200 km altitude was considered because the focus was to decrease ΔV_{dep}. Thus, considering other Martian orbits or other orbital insertion maneuvers at Mars (e.g. aerobraking or aerocapture) can lower ΔV_{tot} even further. Another consideration is that the analysis developed to create the results presented in this paper can easily

be used to develop departure DRO maneuvers to achieve other desired C_3 to target other celestial bodies.

DROs may serve a broader role than "simply" helping in human Mars exploration. Figure 16 presents a ΔV road map showing the advantageous role of having a "refueling depot" in a DRO for various mission scenarios. The ΔV values provided (in km/s) are minimum ΔV estimates based on the assumption of impulsive maneuvers.

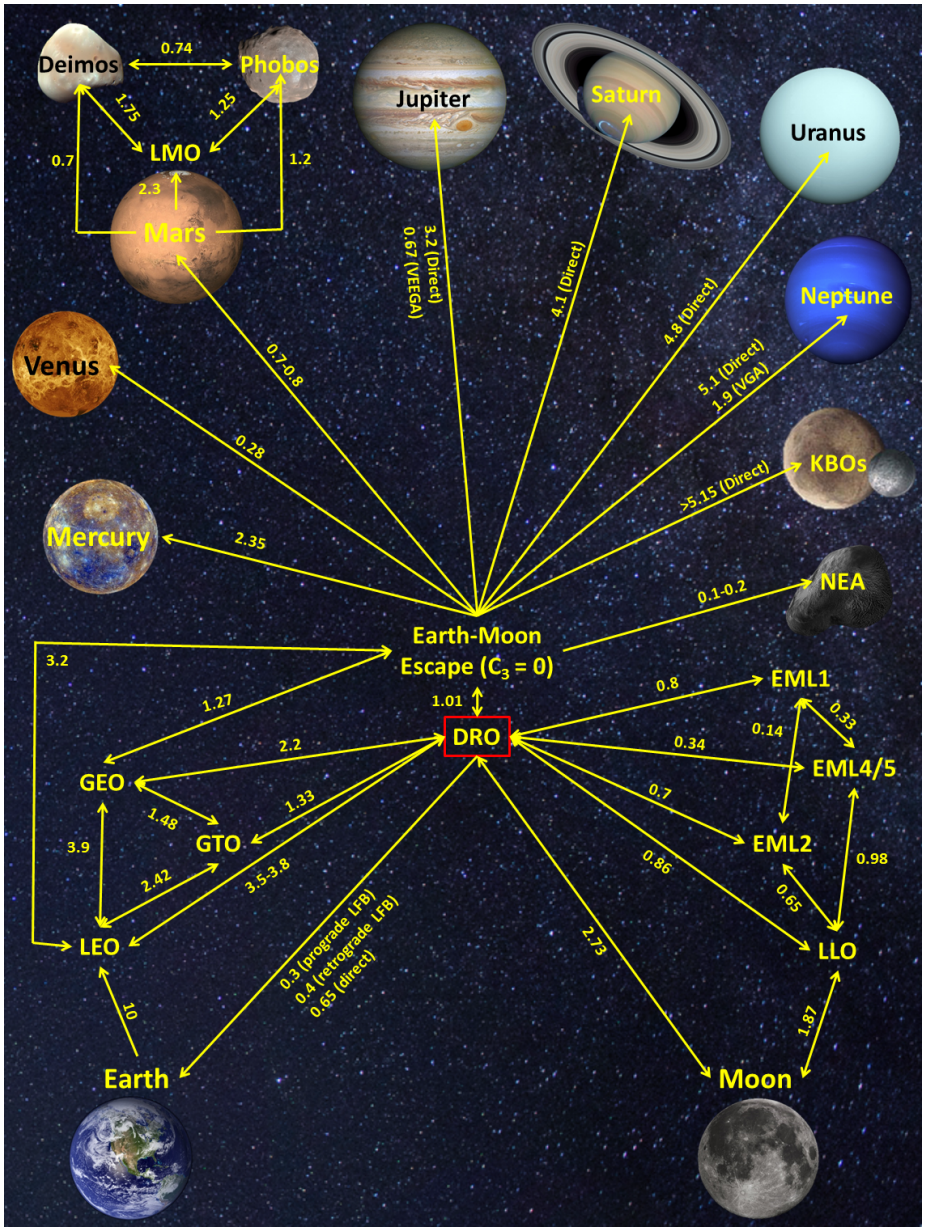

Figure 16: ΔV road map showing the role of a sample DRO (amplitude of 61,500 km) for cis-lunar and deep space missions. All values are in km/s; LFB = Lunar Flyby. [16, 20, 21, 22, 23, 13, 24].

6. Acknowledgment

The authors would like to thank the California Institute of Technology and the Caltech Space Challenge 2015 organizers, mentors and staff members. In March 2015, Davide, Marilena, and Koki were given the opportunity to work together in the 2015 Caltech Space Challenge and exploit the advantages of using a lunar DRO for future space exploration. This paper shows how an asteroid in a DRO could be mined for propellant and used to facilitate human missions to Mars.

References

[1] K. Ho, O. L. de Weck, J. A. Hoffman, R. Shishko, Dynamic modeling and optimization for space logistics using time-expanded networks, Acta Astronautica 105 (2) (2014) 428–443. doi:10.1016/j.actaastro.2014.10.026.

[2] D. Arney, A. Wilhite, Orbital propellant depots enabling lunar architectures without heavy-lift launch vehicles, Journal of Spacecraft and Rockets 47 (2) (2010) 353–360. doi:/10.2514/1.44532.

[3] K. Ho, K. Gerhard, A. K. Nicholas, A. J. Buck, J. Hoffman, On-orbit depot architectures using contingency propellant, Acta Astronautica 96 (2014) 217–226. doi:10.1016/j.actaastro.2013.11.023.

[4] J. Wilson, NASA's Journey to Mars, https://www.nasa.gov/topics/journeytomars/index.html, Accessed: 2016-04-01.

[5] European Space Agency, Moon Village: Humans and Robots Together on the Moon., http://www.esa.int/About_Us/DG_s_news_and_views/Moon_Village_humans_and_robots_together_on_the_Moon, Accessed: 2016-04-01.

[6] K. Hambleton, Deep Space Gateway to Open Opportunities for Distant Destinations, https://www.nasa.gov/feature/deep-space-gateway-

to-open-opportunities-for-distant-destinations, Accessed: 2017-04-05.

[7] P. Troutman, D. Mazanek, F. Stillwagen, J. Antol, T. Sarver-Verhey, D. Chato, R. Saucillo, D. Blue, W. Siegfried, D. Carey, S. Krizan, Orbital Aggregation and Space Infrastructure Systems (OASIS), in: 53rd International Astronautical Congress, Houston, TX, 2002.

[8] R. G. Merrill, D. Komar, M. Qu, J. Chrone, N. Strange, D. Landau, An initial comparison of selected Earth departure options for solar electric propulsion missions, in: 2012 IEEE Aerospace Conference, 2012. doi:10.1109/AERO.2012.6187266.

[9] C. Bezrouk, J. Parker, Long Duration Stability of Distant Retrograde Orbits, in: AIAA/AAS Astrodynamics Specialist Conference, AIAA SPACE Forum, San Diego, CA, 2014. doi:10.2514/6.2014-4424.

[10] G. L. Condon, J. Williams, Asteroid Redirect Crewed Mission Nominal Design and Performance, in: SpaceOps 2014 Conference, 5-9 May 2014, Pasadena, CA. doi:10.2514/6.2014-1696.

[11] D. A. Vallado, W. D. McClain, Fundamentals of astrodynamics and applications, Springer Science & Business Media, 2001.

[12] B. Drake, Human exploration of Mars, design reference architecture 5.0, Tech. rep., NASA (2009).
URL https://www.nasa.gov/pdf/373665main_NASA-SP-2009-566.pdf

[13] M. Landgraf, M. Düring, F. Renk, Mission Design Aspect of European Elements in the International Space Exploration Framework, in: 24th International Symposium on Space Flight Dynamics, Laurel, Maryland, 2014.

[14] V. Boccia, D. Conte, S. Dandavino, P. Das, T. de Roche, M. Di Carlo, D. Fries, R. Goel, K. Ho, H. Jethani, M. Khatsenko, M. Lapotre, A. Morita, B. Tandy, L. Wilson, L-DORADO: Lunar - reDirected Orbiting Resource

Asteroid Demonstration and Operation, Presented at the California Institute of Technology Space Challenge, March 2015.

[15] E. A. Belbruno, J. K. Miller, Sun-perturbed Earth-to-Moon transfers with ballistic capture, Journal of Guidance, Control, and Dynamics 16 (4) (1993) 770–775. doi:10.2514/3.21079.

[16] L. Capdevila, D. Guzzetti, K. Howell, Various Transfer Options from Earth into Distant Retrograde Orbits in the Vicinity of the Moon, in: 24th AAS/AIAA Space Flight Mechanics Meeting, Santa Fe, NM, 2014.

[17] J. Williams, G. L. Condon, Contingency Trajectory Planning for the Asteroid Redirect Crewed Mission, in: SpaceOps Conference, 5-9 May 2014, Pasadena, CA, 2014.

[18] NOA, NOAA Solar Calculator, https://www.esrl.noaa.gov/gmd/grad/solcalc/celsphere.gif, Accessed: 2017-03-20.

[19] D. Conte, Determination of Optimal Earth-Mars Trajectories to Target the Moons of Mars, Master's thesis, The Pennsylvania State University (2014).

[20] W. J. Larson, L. Prankle, in: Human Spaceflight: Mission Analysis and Design, McGraw-Hill Companies, 1999.

[21] J. W. Wertz, D. F. Everett, J. J. Puschell, Space Mission Engineering: The New SMAD, Vol. 28, Space Technology Library, 2011.

[22] F. Renk, Investigation on Low Cost Transfer Options to the Earth-Moon Libration Point Region, Master's thesis, University of Stuttgart (2009).

[23] B. Barbee, Near Earth Object Program, http://neo.jpl.nasa.gov/nhats/, Accessed: 2017-04-01.

[24] D. I. Fiehler, S. R. Oleson, Neptune Orbiters Utilizing Solar and Radioisotope Electric Propulsion, in: 2004 AIAA Aerospace Conference, AIAA, 2004.